Synthesis of a Rod-Based Porous Coordination Polymer from a Nucleotide as Sequential Chiral Inductor.

Rosaria Bruno, [a] Teresa F. Mastropietro,[a] Giovanni De Munno, Emilio Pardo[b] and Donatella Armentano[c]

[c]*Dipartimento di Chimica e Tecnologie Chimiche, Università della Calabria, 87030 Rende, Cosenza, Italy.* [b]*Institut de Ciencia Molecular (ICMol), Universitat de Valencia, 46980 Paterna, Valencia, Spain.*

Synthesis of a Rod-Based Porous Coordination Polymer from a Nucleotide as Sequential Chiral Inductor.

We report the two-step synthesis of a novel chiral rod-based porous coordination polymer (PCP). The chemical approach consists on the use of a previously prepared bis(ethylendiamine) copper monomer of formula $[Cu(en)]_2(NO_3)_2$ [where en = ethylendiamine] reacting with the cytidine 5'-monophosphate (CMP) nucleotide. The bis(ethylendiamine) copper compound –stabilized by the axial coordination of nitrate counter-anions– reacts in the presence of sodium salt of CMP to yield right-handed copper(II) chains of *P* helicity with formula $[Cu_2(en)_2(CMP)_2] \cdot 5H_2O$ (**1**). The axial coordination of the CMP^{2-} ligands through the N3 and O2 sites (free nitrogen and carbonyl groups) of the cytosine nucleobase and oxygen atoms of phosphate moieties, ensure the stabilization of the neutral chiral polymer. The supramolecular organization involves strong hydrogen bonding interactions to build supramolecular chains of the same helicity. The resulting PCP constitutes one of the few examples of CMP compounds exhibiting a such coordination involving both nucleobase and phosphate moieties, where a highly stable metal complex is used as precursor for the rational construction of rod-based hydrogen metal-organic frameworks (HMOFs). Furthermore, it is underlined the intrinsic capability of biomolecules to act as chiral transfer systems.

1. Introduction

Metal-organic frameworks (MOFs)[1,2] and covalent-organic frameworks (COFs)[3,4] are a kind of crystalline porous materials featuring well-defined channels with predefined functionality. Their intrinsic porosity and rich host-guest chemistry are at the origin of fascinating properties.[5] Indeed, MOFs and COFs find application in fields as diverse as gas storage and separation,[6] catalysis,[3,7,8] magnetism,[9–11] transport,[12–14] and sensing,[15] drug delivery,[16] and water remediation.[17,18]

Recently, an emerging class of porous materials known as hydrogen-bonded organic frameworks (HOFs) and hydrogen-bonded metal-organic frameworks (HMOFs) – generally included in HOFs – have attracted increasing attention.[19] They exploit hydrogen-bonding interactions to build porous structures from pure organic or metal-containing organic building blocks. Despite, the apparent lack of robustness for the vast majority of HMOFs –which often collapse upon removal of the solvent molecules in the voids– several HMOFs, exhibiting permanent porosity, have already been reported.[20,21]

Despite the mentioned drawback, HMOFs exhibit several inherent advantages, in terms of cost, purification, regeneration and potential water tolerance.[19,20,22] Furthermore, weak hydrogen bonds, even if responsible for the frequent instability, make them rather more flexible than materials based on covalent and coordination bonds. However, only

very few HMOFs have demonstrated both permanent porosity and intriguing dynamic behaviors. Overall, HMOFs are very promising materials for the sensing, capture and separation, but much work remains to be done in order to achieve a real application and, specially, to fully understand how to exploit in a judicious way the interactions that govern the supramolecular self-assembly processes. In this context, rod-based HMOFs, that are porous supramolecular coordination polymers based on infinite one-dimensional (1D) rod-based building units (SBUs), hydrogen bonded to build the 3D frameworks, may be promising candidates, as they may increase robustness of the final material. In this context, it is clear that the development of novel examples of rod-based HMOFs would be highly desirable to move toward the establishment of rational design methodologies of rod-HMOFs as well as the formation mechanisms involved.

The use of chiral molecules from bio-world, intrinsically devoted to stabilize supramolecular species *via* hydrogen bonds, can lead to both flexibility and chirality in the final framework.[23,24] Among others nucleotide and nucleoside, in principle, are suitable candidates to combine soft hydrogen bonding, robustness ensured by phosphate coordination and chirality to get flexible building blocks.[25–27] They could potentially realize, based on chemical affinity of sugar moiety and size or shape-selectivity effects of the final networks, multimode structural transformations in response to appropriate physical or chemical external stimuli.[28] It has been well established that only enantiopure building blocks ensures that the encoded chiral information enclosed on them is transferred to the final polymeric structure, which features both chiral voids where chiral active sites are available for example for the enantioselective recognition. Indeed, such materials are, potentially the best candidates to carry out efficiently separation of enantiomers.[28,29]

Following our recent work concerning the use of nucleosides[26][25][30] or nucleotides[28,29,31] as precursors to construct a variety of chiral clusters and chiral coordination polymers, we have prepared, in a two-step synthesis, a novel one-dimensional chiral rod-based coordination polymer using cytidine 5'-monophosphate (CMP) nucleotide of formula $[Cu_2(en)_2(CMP)_2] \cdot 5H_2O$ (**1**), (en = ethylendiamine). The reaction and reorganization of the mononuclear precursor $[Cu(en)]_2(NO_3)_2$ in the presence of CMP (in acidic media) yields the final neutral rod-based polymer (Scheme 1). Noteworthy, the intrinsic capability of CMP nucleoside to act as sequential chiral inducer, is pretty disclosed on the final supramolecular organization, where strong hydrogen bonds assemble chains giving rise to right-handed helices.

2. Experimental Section

2.1. Materials

All reagents were purchased from commercial sources and used as received. $[Cu(en)]_2(NO_3)_2$ was prepared as previously reported.[32]

2.2. Synthesis of compound (1).

$[Cu_2(en)_2(CMP)_2] \cdot 5H_2O$ (1). Synthesis of **2** was carried out by direct reaction of water:ethanol (9:1 v/v) solutions of compound $[Cu(en)]_2(NO_3)_2$ and the sodium salt of CMP (Na_2CMP) at pH = 4: 10 mL of the $[Cu(en)]_2(NO_3)_2$ solution adjusted a pH = 4 (xxx mg, 2 mmol) was added dropwise over 10 mL of aqueous solution containing Na_2CMP

(xxx mg, 4 mmol). The resulting mixture was stirred for 30 minutes and then, the precipitated green polycrystalline powder was filtered off and air-dried. Yield: xx mg, 75 %; Anal.: calcd. for $C_{22}H_{50}Cu_2N_{10}O_{21}P_2$ (979.73): C, 26.97; H, 5.14; N, 14.30. Found: C, 26.01; H, 5.06; N, 14.52%; IR (KBr): ν = 1610 cm^{-1} (C=O).
Well-formed blue parallelepipeds of **1**, suitable for X-ray diffraction, could also be obtained by slow diffusion in an H-shaped tube of stoichiometric amounts of $[Cu(en)]_2(NO_3)_2$ dissolved at pH = 4 and Na_2CMP in each arm of the tube, using the same water/ethanol solvent. The crystals were collected by filtration and air-dried.

2.3. Physical Techniques

Elemental analyses (C, H, N) were performed at the microanalysis service of the Dipartimento di Chimica e Tecnologie Chimiche, of the Università della Calabria (Italy). The FTIR spectra were recorded on a Nicolet-6700 spectrophotometer as KBr pellets. The UV-Vis spectra were recorded on a Nicolet Evolution 600 spectrophotometer. The thermogravimetric analysis was performed on crystalline samples under a dry N_2 atmosphere with a Perkin-Elmer equipment with thermobalance operating at a heating rate of 10 ºC min^{-1}.

2.4 X-ray Powder Diffraction Measurements

A polycrystalline sample of **1** was deposited on a flat plate of 5 cm as diameter prior to being mounted on a Bruker D2 PHASER Diffraction System with Cu-Kα radiation (λ = 1.54056 Å). Five repeated measurements were collected at room temperature (2θ = 2–50°) and merged in a single diffractogram.

2.5 Crystal Structure Data Collection and Refinement

A crystal with *ca*.0.24 x 0.20 x 0.18 mm as dimensions, was selected and mounted on a MITIGEN holder in Paratone oil under a nitrogen stream at a temperature of 100 K. The sample is perfectly stable at air and room temperature. Low temperature acquisition data was performed in order to reduce solvent thermal disorder. Diffraction data were collected on a Bruker-Nonius X8APEXII CCD area detector diffractometer using graphite-monochromated Mo-K_α radiation (λ = 0.71073 Å). The data were processed through SAINT[33] reduction and SADABS[34] multi–scan absorption software. The structures were solved with the SHELXS structure solution program, using the Patterson method. The model was refined with version 2018/3 of SHELXL against F^2 on all data by full–matrix least squares.[35,36]
All non-hydrogen atoms were refined with anisotropic displacement parameters. The lattice solvent molecules were still thermally disordered, residing in accessible voids featured by **1**. They were anyway confirmed by thermogravimetric and elemental analysis and correctly reported in final formula. The hydrogen atoms of the ligands were set in calculated positions and refined as riding atoms whereas for water molecules were found form ΔF maps and then refined with O-H and H-H distance restrains.
Without found solvent molecules, the effective free volume of **1** is calculated by PLATON analysis to be 11.4 % of the crystal volume (212.1 of the 1853.8 $Å^3$ of the unit cell volume). In accordance with SCXRD analysis, the voids of **1** are entirely filled by solvent guests.
A summary of the crystallographic data and structure refinement for **1**-**2** is given in Table 1. CCDC reference number is XXXXXXX.

The comments for the alerts B are described in the CIFs using the validation response form (vrf).

The final geometrical calculations on free voids and the graphical manipulations were carried out with PLATON[37,38] implemented in WinGX,[39,40] and CRYSTAL MAKER[41] programs, respectively.

3. Results and Discussion

3.1 Powder X-ray diffraction and Thermo-gravimetric analysis

In order to confirm the purity of the polycrystalline sample and its isostructurality with the crystal selected for single-crystal X-ray diffraction, the PXRD pattern of a polycrystalline sample of **1** was measured showing that crystallinity is retained when exposed to the air at room temperature and even after the sample was left at 60 °C for 24 h (Figures 1b and 1c). This situation reveals that the framework of **1** does not easily collapse upon removal of water molecules. The experimental PXRD pattern profiles (Figures 1b and 1c) are consistent with the calculated one (Figure 1a), confirming that the bulk sample is isostructural to the crystal selected for single-crystal X-ray diffraction.
The water contents of **1** was confirmed by thermogravimetric analysis (TGA) under a dry N_2 atmosphere. A moderate mass loss from room temperature to around 100 °C can be observed in Figure 2. It is followed by a *plateau* in the range 100-150 °C, when decomposition starts. The value of the mass loss at around 100 °C of *ca*. 9 % corresponds with 5 water molecules per formula unit.

3.2 Crystal structure

The well-formed blue parallelepiped crystals of **1** allowed us to carry out single crystal X-ray diffraction measurement and the resolution of its crystal structure. Compound **1** crystallizes in the chiral space group $P2_1$ of the monoclinic system. The 3D framework of **1** is built by supramolecular chiral double-chains of *P* handness, interconnected through strong hydrogen bonding interactions (Figures 3-11), which hold $\{[Cu_2(en)_2(CMP)_2\}_n$ chains by interacting free hydrophilic hydroxyl groups from the ribose units, pointing towards the voids, and oxygen atoms of phosphate moieties from the CMP nucleotide. These interconnected chains growing along *b* axis are stacked by weak but efficient hydroxyl-alkyl interactions ensured by ribose moieties and ethylendiammine ligands (Figures 6). The resulting functional voids enclose hydrophilic hydroxyl groups from the ribose units, pointing towards the holes (Figures 7-8). Lattice water molecules reside within these functional holes (Figure 7-8).

The asymmetric unit contains two distinct copper ions, two ethylendiammine and two CMP ligands, coordinated as bridges through the oxygen atoms of the phosphate groups and *via* N(3) and exocyclic O(2) of the nucleobase (Figure 3). Couples of μ_2-phosphate groups connect two crystallographically independent copper(II) ions, giving rise to very robust dinuclear cores of the type $[Cu_2(\mu_2\text{-}PO_4)_2]$ decorated by terminal ethylendiammine ligands. The additional coordination of CMP *via* N(3)/O(2) atoms of the pyrimidine base towards Cu(II) ions assures the growth of the chain (Figures 3 and 4). The simultaneous coordination of CMP *via* N(3)/O(2) atoms and phosphate groups towards distinct copper

ions joining two dinuclear cores [$Cu_2(\mu_2\text{-}PO_4)_2$] produces a double enlace of copper ions within the chain (Figures 3 and 4). This coordination mode is likely at the origin of the outstanding stability observed (Figures 1 and 2).

The two crystallographically distinct copper ions exhibit six-coordinated distorted axially elongated octahedral environments (Figure 3). They are formed by one chelating en ligand, two oxygen atoms from two distinct phosphates of CMP and one hooking cytosine nucleobase. The orientation of the nucleobase rings is such to place the carbonyl pointing toward the copper atoms, with its oxygen atom occupying the axial positions at a distance of 2.801(7) and 2.845(7) Å, for Cu(1) and Cu(2), respectively (Table S1). The equatorial and axial Cu–$O_{phosphate}$ lengths are 1.979(7) and 2.340(7) for Cu(1) and 1.946(7) and 2.339(7) Å for Cu(2) whereas the Cu-N bond lengths fall in the ranges 1.999(8) - 2.049(7) Å (Table S1).

Concerning the chemical and chiral nature of the functional voids, the sugar moieties of the CMP ligands, pointing within the holes of the net, exhibit the C(2′) – *endo* conformation whereas the conformation of the C(4′) - C(5′) is *trans-gauche*. Their chiral centers at C1′, C2′, C3′ and C4′ have configuration *R, R, S, R* (Scheme 1). As anticipated above, chains are joined by strong and symmetric hydrogen bonding interactions involving hydroxyl groups from ribose of one chain with oxygen atoms from phosphate of another chain (Figure 5 and Table S3) [O-H ⋯ O 1.86(1) and 1.84(1) and O⋯O of 2.68(1) Å]. As made couple of chains built supramolecular helices growing along *b* axis of *P* handness, underlining how encoded chirality of building blocks is transferred to the supramolecular motif (Figures 9-10). Further insights into the structure of **1** can be gained by reducing structure to simple copper rod geometries. As shown in Figure 5, the {[$Cu_2(en)_2(CMP)_2$}$_n$ chains, are connected via hydrogen bonds to construct a 2_1 helix. Then these two-fold helices of *P* handness are packed via further interactions to generate a porous 3D HMOF (Figure 9). These right-handed helices (Figure 11) with helical pitch of 13.259 Å (of course the *b* axis value) are joined by means of weak interactions established between hydroxyl groups and alkyl residues of ethylendiammine pointing towards voids, of the type H-O⋯H-C [O⋯H distance of 2.36(1) Å, Figure 6 and Table S2]. Intercalated between helices reside lattice water molecules to stabilize the 3D network via an intricate network of hydrogen bonds (Figure 7-10 and Table S2). Indeed, strong hydrogen bonds interconnecting lattice water molecules to ribose and phosphate of CMP nucleotide generate a 3D chiral porous network viewed along the [010] direction (Figure 8). Taking van der Waals radii into account, without found solvent molecules, the effective free volume, entirely filled by solvent guests of **1**, is calculated to be 11.4 % of the crystal volume (212.1 of the 1853.8 $Å^3$ of the unit cell volume). Noteworthy, as shown in Figure 2, compound **1** exhibit an outstanding stability even upon water removal making it a promising material for separation and sensing applications. We are aware that available holes are small in size (Figure 8) but it could be an advantage for enantiomeric separation of small chiral molecules that actually is still challenging given two given enantiomers show identical chemical and physical properties in achiral environments. Chiral recognition appears as the only good strategy to achieve such objective.

It is also worth to note that, despite the similarity of coordination mode of CMP in **1** and compounds of formulae [$Cu_7(phen)_6(CMP)_4$] · $(NO_3)_6$ · $(H_2O)_{46}$ (**1**), (phen = 1,10 phenanthroline)[29] and {[$Cu_5(bpy)_5(OH)(H_2O)_2(CMP)_2(ClO_4)$]$(ClO_4)_4$·$9H_2O$}$_n$,[28] previously reported by us and both prepared using nucleotide as chiral inducer and α-diimine as terminal ligands, self-assembling of each chiral brick occurs in different manner linking copper chains in a very different fashion. This is likely a direct

consequence of diverse chemistry of aromatic versus aliphatic α-diimine ligands where dissimilar supramolecular interactions, π···π stacking for instance, not allowed in **1**, govern the overall nature of the final material.

4. Conclusions

In summary, we report the preparation and characterization of a new chiral rod-based hydrogen metal-organic framework (HMOF) following a dual-step synthetic process. The synthetic approach consists on the use of a previously prepared bis(ethylendiamine) copper monomer capable to rearrange and reassemble forming copper(II) rods in the presence of cytidine 5'-monophosphate (CMP) nucleotide. CMP intrinsic nature to molecular recognition –by means of hydrogen bonding– yields very robust right-handed copper(II) supramolecular chains of *P* helicity. Present work reports one of the very few examples where a nucleotide is used for the rational construction of a rod-based HMOFs. Robustness of the final material together with its not negligible porosity, make **1** a promising material for chiral separation. A joint analysis of this work and other previously reported works suggest that the intrinsic nature and chemical affinity of natural nucleotides can be fruitfully exploited to transfer encoded chirality to the final network *via* a self-assembling process, which is mainly governed by supramolecular interactions. Furthermore, the size and shape of the voids, hosting hydrophilic ribose residues from the nucleotide, permit supplementary supramolecular interactions such as π···π ones, that can be somehow tuned by ancillary ligands, and can be helpful to the rational design of 'appropriate holes' in terms of size and shape to hold a given family of small molecules.

5. Acknowledgements

This work was supported by the Ministero dell'Università e della Ricerca. D.A. and R.B. acknowledges the financial support of the Fondazione CARIPLO / "Economia Circolare: ricerca per un futuro sostenibile" 2019, Project code: 2019–2090, MOCA. E.P. acknowledges the financial support of the European Research Council under the European Union's Horizon 2020 research and innovation programme / ERC Grant Agreement No 814804, MOF–reactors.

6. References

[1] H. Deng, C. J. Doonan, H. Furukawa, R. B. Ferreira, J. Towne, C. B. Knobler, B. Wang, O. M. Yaghi, *Science* **2010**, *327*, 846–850.

[2] H. Furukawa, K. E. Cordova, M. O'Keeffe, O. M. Yaghi, *Science* **2010**, *9*, 1230444.

[3] A. G. Slater, A. I. Cooper, *Science* **2015**, *348*, 988-.

[4] S. Lin, C. S. Diercks, Y.-B. Zhang, N. Kornienko, E. M. Nichols, Y. Zhao, A. R. Paris, D. Kim, P. Yang, O. M. Yaghi, et al., *Science* **2015**, *1*, 1–11.

[5] H.-C. J. Zhou, S. Kitagawa, *Chem. Soc. Rev.* **2014**, *43*, 5415–5418.

[6] C. Wang, D. Liu, W. Lin, *J. Am. Chem. Soc.* **2013**, *135*, 13222–13234.

[7] K. Kratzl, T. Kratky, S. Günther, O. Tomanec, R. Zbořil, J. Michalička, J. M. Macak, M. Cokoja, R. A. Fischer, *J. Am. Chem. Soc.* **2019**, *141*, 13962–13969.

[8] F. R. Fortea-Pérez, M. Mon, J. Ferrando-Soria, M. Boronat, A. Leyva-Pérez, A. Corma, J. M. Herrera, D. Osadchii, J. Gascon, D. Armentano, et al., *Nat. Mater.* **2017**, *16*, DOI 10.1038/nmat4910.

[9] J. Vallejo, F. R. Fortea-Pérez, E. Pardo, S. Benmansour, I. Castro, J. Krzystek, D. Armentano, J. Cano, *Chem. Sci.* **2016**, *7*, DOI 10.1039/c5sc04461h.

[10] M. Mon, A. Pascual-Álvarez, T. Grancha, J. Cano, J. Ferrando-Soria, F. Lloret, J. Gascon, J. Pasán, D. Armentano, E. Pardo, *Chem. Eur. J.* **2016**, *22*, DOI 10.1002/chem.201504176.

[11] A. J. Howarth, A. W. Peters, N. A. Vermeulen, T. C. Wang, J. T. Hupp, O. K. Farha, *Chem. Mater.* **2017**, *29*, 26–39.

[12] X. Han, J. Huang, C. Yuan, Y. Liu, Y. Cui, *J. Am. Chem. Soc.* **2018**, *140*, 892–895.

[13] T. Grancha, J. Ferrando-Soria, J. Cano, P. Amoros, B. Seoane, J. Gascon, M. Bazaga-Garcia, E. Losilla, A. Cabeza, D. Armentano, et al., *Chem. Mater.* **n.d.**, *28*, 4608–4615.

[14] C. Doonan, R. Riccò, K. Liang, D. Bradshaw, P. Falcaro, *Acc. Chem. Res.* **2017**, *50*, 1423–1432.

[15] J. Zhu, P. Z. Li, W. Guo, Y. Zhao, R. Zou, *Coord. Chem. Rev.* **2018**, *359*, 80–101.

[16] Y. Liu, Y. Zhao, X. Chen, *Theranostics* **2019**, *9*, 3122–3133.

[17] M. Mon, R. Bruno, J. Ferrando-Soria, D. Armentano, E. Pardo, *J. Mater. Chem. A* **2018**, DOI 10.1039/C8TA00264A.

[18] J. E. Efome, D. Rana, T. Matsuura, C. Q. Lan, *J. Mater. Chem. A* **2018**, *6*, 4550–4555.

[19] P. Li, M. R. Ryder, J. F. Stoddart, *Accounts Mater. Res.* **2020**, DOI 10.1021/accountsmr.0c00019.

[20] B. Wang, R. He, L. H. Xie, Z. J. Lin, X. Zhang, J. Wang, H. Huang, Z. Zhang, K. S. Schanze, J. Zhang, et al., *J. Am. Chem. Soc.* **2020**, *142*, 12478–12485.

[21] W. Yang, A. Greenaway, X. Lin, R. Matsuda, A. J. Blake, C. Wilson, W. Lewis, P. Hubberstey, S. Kitagawa, N. R. Champness, et al., *J. Am. Chem. Soc.* **2010**, *132*, 14457–14469.

[22] Q. Huang, W. Li, Z. Mao, L. Qu, Y. Li, H. Zhang, T. Yu, Z. Yang, J. Zhao, Y. Zhang, et al., *Nat. Commun.* **2019**, *10*, 1–8.

[23] J. Navarro-Sánchez, A. I. Argente-García, Y. Moliner-Martínez, D. Roca-Sanjuán, D. Antypov, P. Campíns-Falcó, M. J. Rosseinsky, C. Martí-Gastaldo, *J. Am. Chem. Soc.* **2017**, *139*, 4294–4297.

[24] I. Imaz, M. Rubio-Martínez, J. An, I. Solé-Font, N. L. Rosi, D. Maspoch, *Chem. Commun. (Camb).* **2011**, *47*, 7287–7302.

[25] D. Armentano, T. F. Mastropietro, M. Julve, R. Rossi, P. Rossi, G. De Munno, *J. Am. Chem. Soc.* **2007**, *129*, 2740–2741.

[26] D. Armentano, N. Marino, T. F. Mastropietro, J. Martínez-Lillo, J. Cano, M. Julve, F. Lloret, G. De Munno, *Inorg. Chem.* **2008**, *47*, 10229–10231.

[27] V. Amendola, G. Bergamaschi, A. Buttafava, L. Fabbrizzi, **2010**, *10*, 147–156.

[28] N. Marino, D. Armentano, E. Pardo, J. Vallejo, F. Neve, L. Di Donna, G. De Munno, *Chem. Sci.* **2015**, *6*, DOI 10.1039/c5sc01089f.

[29] R. Bruno, N. Marino, L. Bartella, L. Di Donna, G. De Munno, E. Pardo, D. Armentano, *Chem. Commun.* **2018**, *54*, DOI 10.1039/c8cc03544j.

[30] N. Marino, D. Armentano, T. F. Mastropietro, M. Julve, F. Lloret, G. De Munno, *Cryst. Growth Des.* **2010**, *10*, 1757–1761.

[31] N. Marino, D. Armentano, C. Zanchini, G. De Munno, *CrystEngComm* **2014**, *16*, DOI 10.1039/c4ce00511b.

[32] V. Manríquez, M. Campos-Vallette, N. Lara, N. González-Tejeda, O. Wittke, G. Díaz, S. Diez, R. Muñoz, L. Kriskovic, *J. Chem. Crystallogr.* **1996**, *26*, 15–22.

[33] SAINT, *Version 6.45; Bruker Analytical X-Ray Systems: Madison, WI*, **2003**.

[34] G. M. Sheldrick, **2003**.

[35] G. M. Sheldrick, *Acta Crystallogr. A.* **2008**, *64*, 112–22.

[36] G. M. Sheldrick, *Acta Crystallogr. Sect. C Struct. Chem.* **2015**, *71*, 3–8.

[37] A. L. Spek, *J. Appl. Crystallogr.* **2003**, *36*, 7–13.

[38] S. Parsons, H. D. Flack, T. Wagner, *Acta Crystallogr. Sect. B Struct. Sci. Cryst. Eng. Mater.* **2013**, *69*, 249–259.

[39] L. J. Farrugia, *J. Appl. Crystallogr.* **1999**, *32*, 837–838.

[40] L. J. Farrugia, *J. Appl. Crystallogr.* **2012**, *45*, 849–854.

[41] D. C. Palmer, *Zeitschrift fur Krist. - Cryst. Mater.* **2015**, *230*, 559–572.

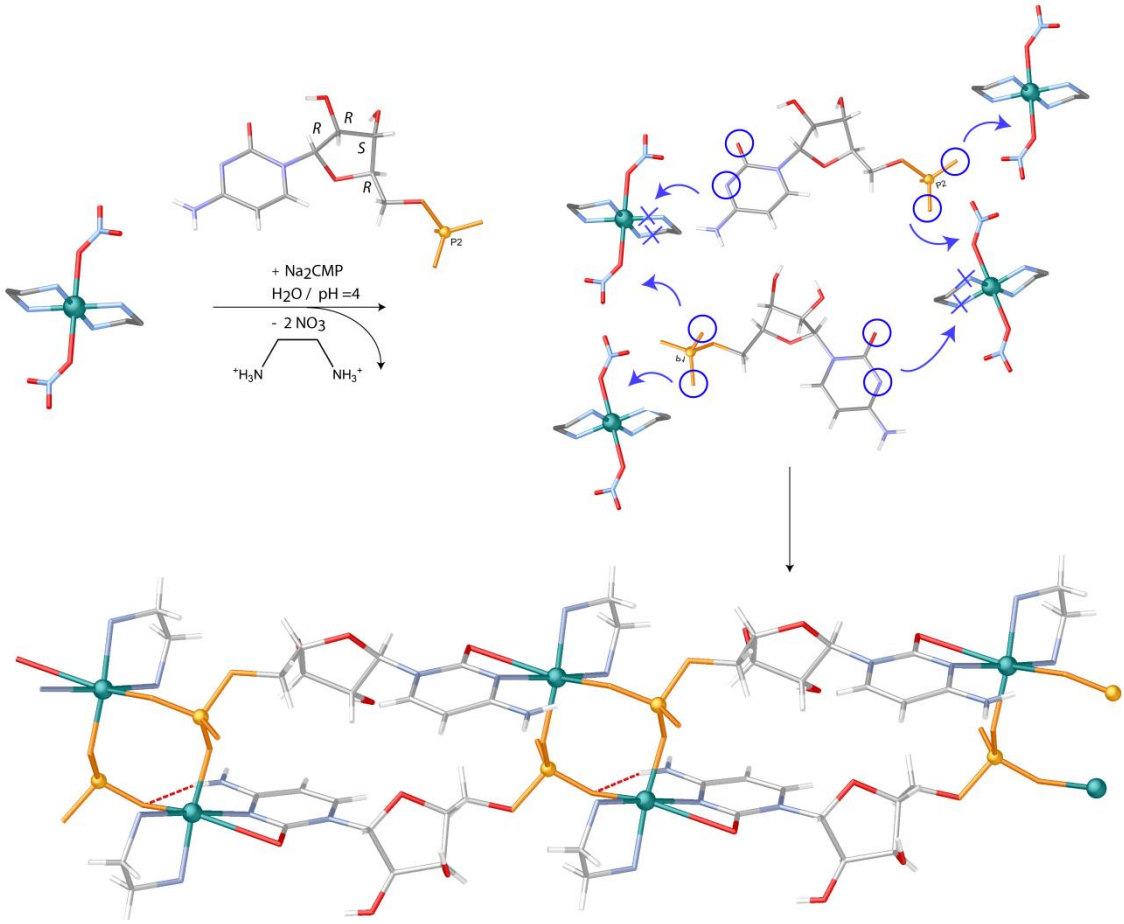

Scheme 1. Hypothetic "metalloligand" approach illustrating the assembly of the chiral 1D structure. View of the $[Cu(en)]_2(NO_3)_2$ and hypothesis of reconstruction process to yield the chain.

Table 1. Summary of Crystallographic Data for **1**.

Compound	**1**
Formula	$C_{22}Cu_2H_{50}N_{10}O_{21}P_2$
M (g mol^{-1})	979.74
λ (Å)	0.71073
Crystal system	Monoclinic
Space group	$P2_1$
a (Å)	8.7130(4)
b (Å)	13.2593(6)
c (Å)	16.2310(8)
α (°)	90
β (°)	98.651(3)
γ (°)	90
V (Å^3)	1853.81(15)
Z	2
ρ_{calc} (g cm^{-3})	1.755
μ (mm^{-1})	1.332
T (K)	100
θ range for data collection (°)	1.992 to 29.788
Completeness to θ = 25.0	98.9 %
Measured reflections	23166
Unique reflections (Rint)	9234 (0.0666)
Observed reflections [$I > 2\sigma(I)$]	8046
[c]Goodness-of-fit on F^2	1.000
Absolute structure parameter (Flack)	0.076(7)
R^a [$I > 2\sigma(I)$] (all data)	0.0710 (0.1990)
wR^b [$I > 2\sigma(I)$] (all data)	0.0794 (0.2058)

[a] $R = \sum(|F_o| - |F_c|)/\sum|F_o|$. [b] $wR = [\sum w(|F_o| - |F_c|)^2/\sum w|F_o|^2]^{1/2}$.

[c] $S = [\sum w(|F_o| - |F_c|)^2/(N_o - N_p)]^{1/2}$.

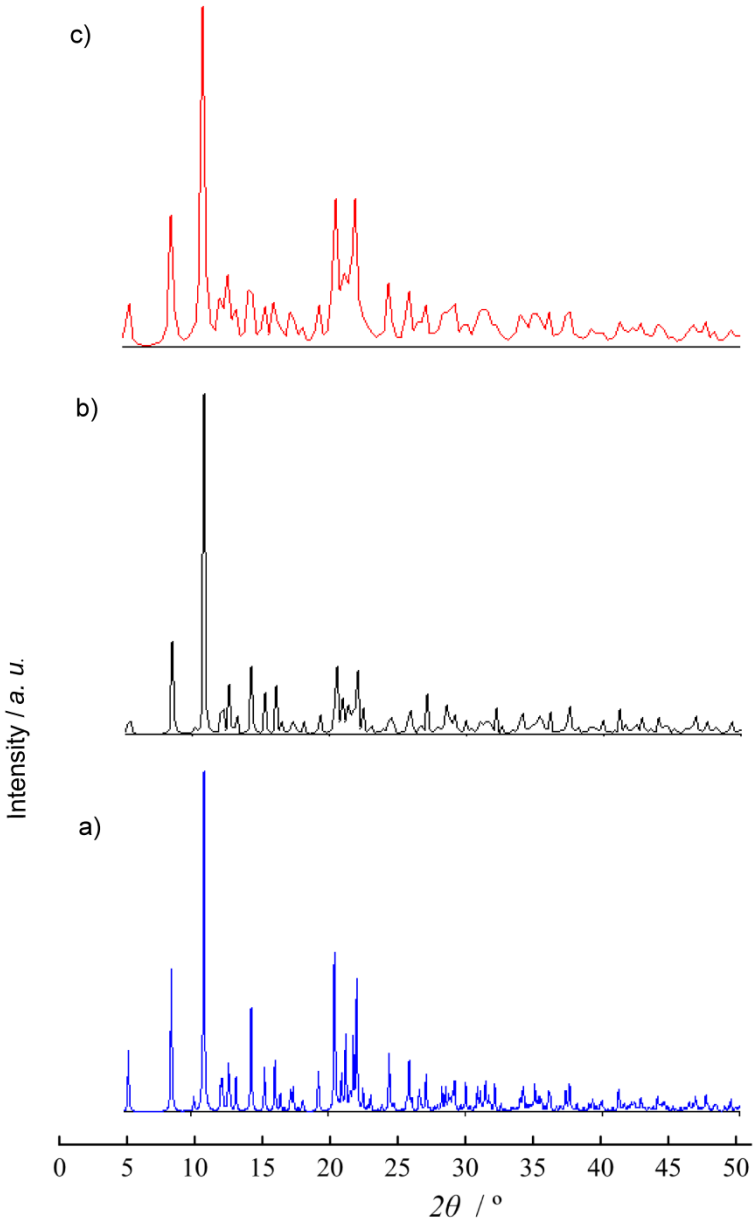

Figure 1. Calculated (a) and experimental PXRD pattern profiles of **2** at room temperature (b) and a polycrystalline evacuated sample (c) of **2**, measured at r.t, in the 2.0–50.0 2θ range.

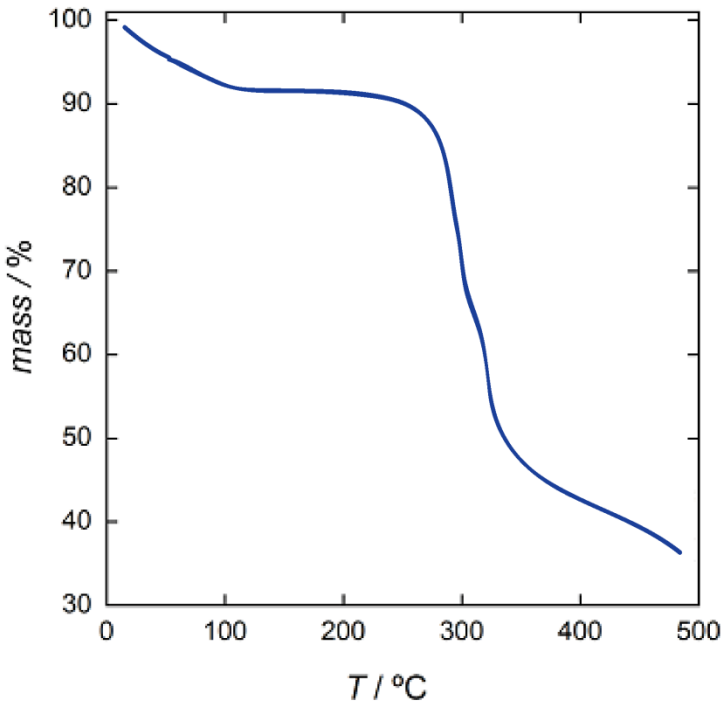

Figure 2. TGA of **2** under dry N_2 atmosphere.

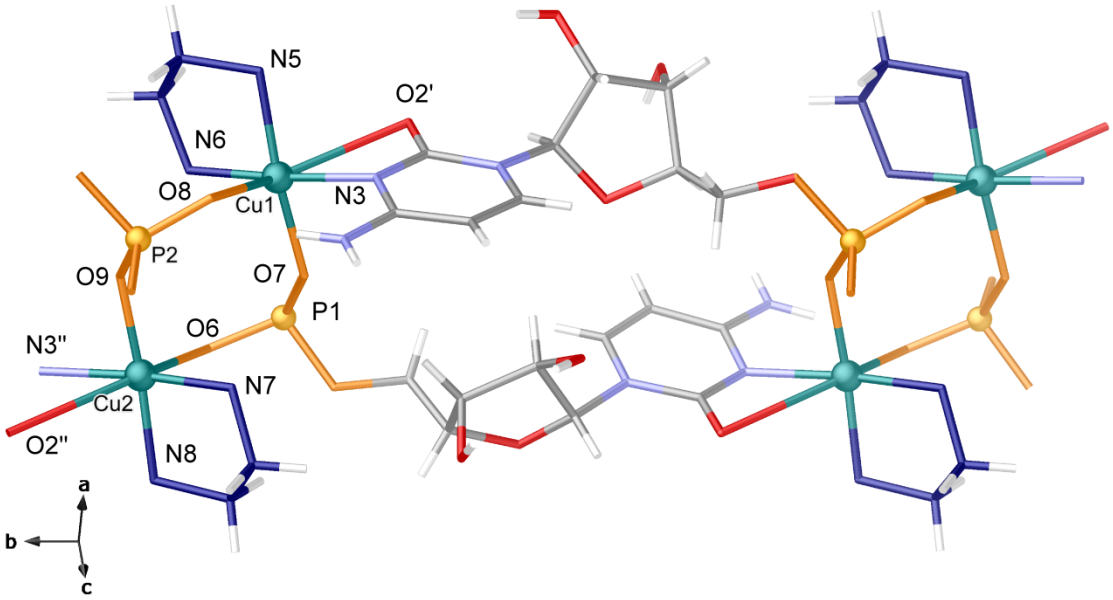

Figure 3. Side views of a portion of $[Cu_2(en)_2(CMP)_2]$ chain of **1** showing the double enlace of copper ensured by CMP together with labelling scheme. The ligands are shown as sticks whereas the copper(II) ions and the phosphorus atoms of the CMP are depicted as green, and gold spheres. Color sticks legend: C, gray; N, light blue; O, red; H, white; Carbon and nitrogen atoms from ethylndiammine ligand have been depicted in blue whereas oxygen atoms of phosphate groups are depicted in gold for the sake of clarity.

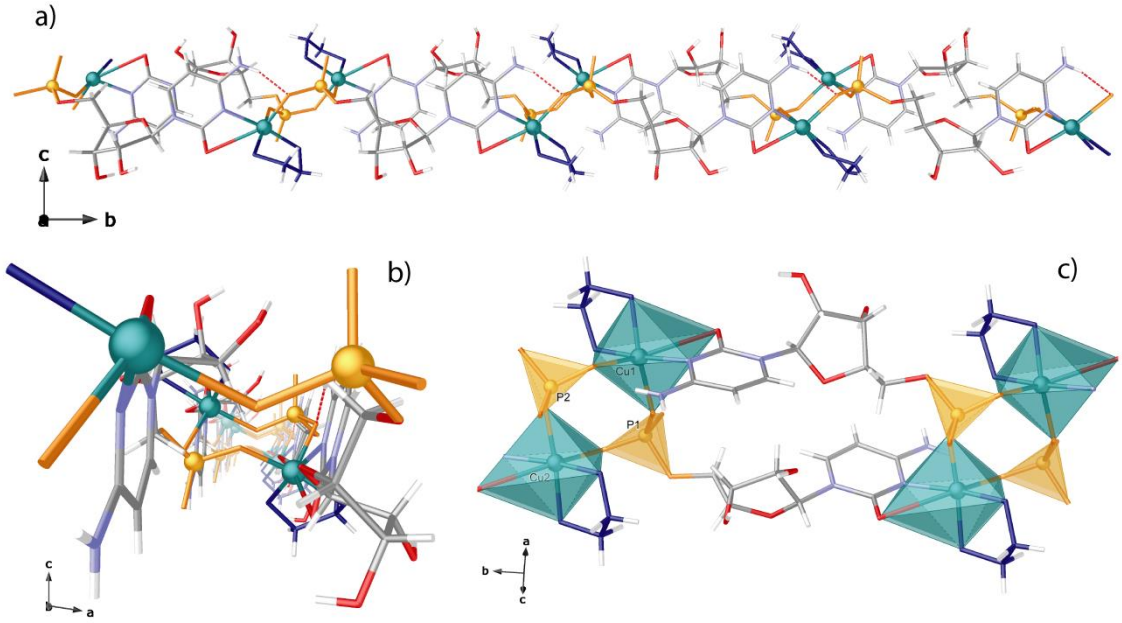

Figure 4. Side (a) and top (b) views of $[Cu_2(en)_2(CMP)_2]$ chains in the crystal structure of **1**. In (c) is underlined the resulting double enlace produced by symmetric coordination of two distinct CMP molecules towards four copper metal ions. The ligands are shown as sticks whereas the copper(II) ions and the phosphorus atoms of the CMP are depicted as green, and gold spheres (except in c where are represented with polyhedral). Color sticks legend: C, gray; N, light blue; O, red; H, white; Carbon and nitrogen atoms from ethylndiammine ligand have been depicted in blue whereas oxygen atoms of phosphate groups are depicted in gold for the sake of clarity.

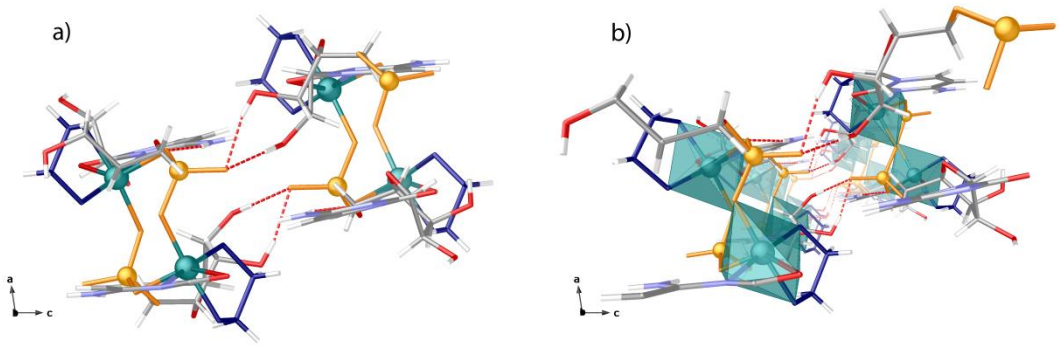

Figure 5. Details without (a) and with perspective (b) of $\{[Cu_2(en)_2(CMP)_2\}_n$ supramolecular chains generated by strong and symmetric hydrogen bonding interactions involving hydroxyl groups from ribose and phosphate from CMP [O-H ⋯ O 1.86(1) and 1.84(1) and O⋯O of 2.68(1) Å]. The ligands are shown as sticks whereas the copper(II) ions and the phosphorus atoms of the CMP are depicted as green, and gold spheres (copper as green polyhedral in b). Color sticks legend: C, gray; N, light blue; O, red; H, white; Carbon and nitrogen atoms from ethylndiammine ligand have been depicted in blue whereas oxygen atoms of phosphate groups are depicted in gold for the sake of clarity.

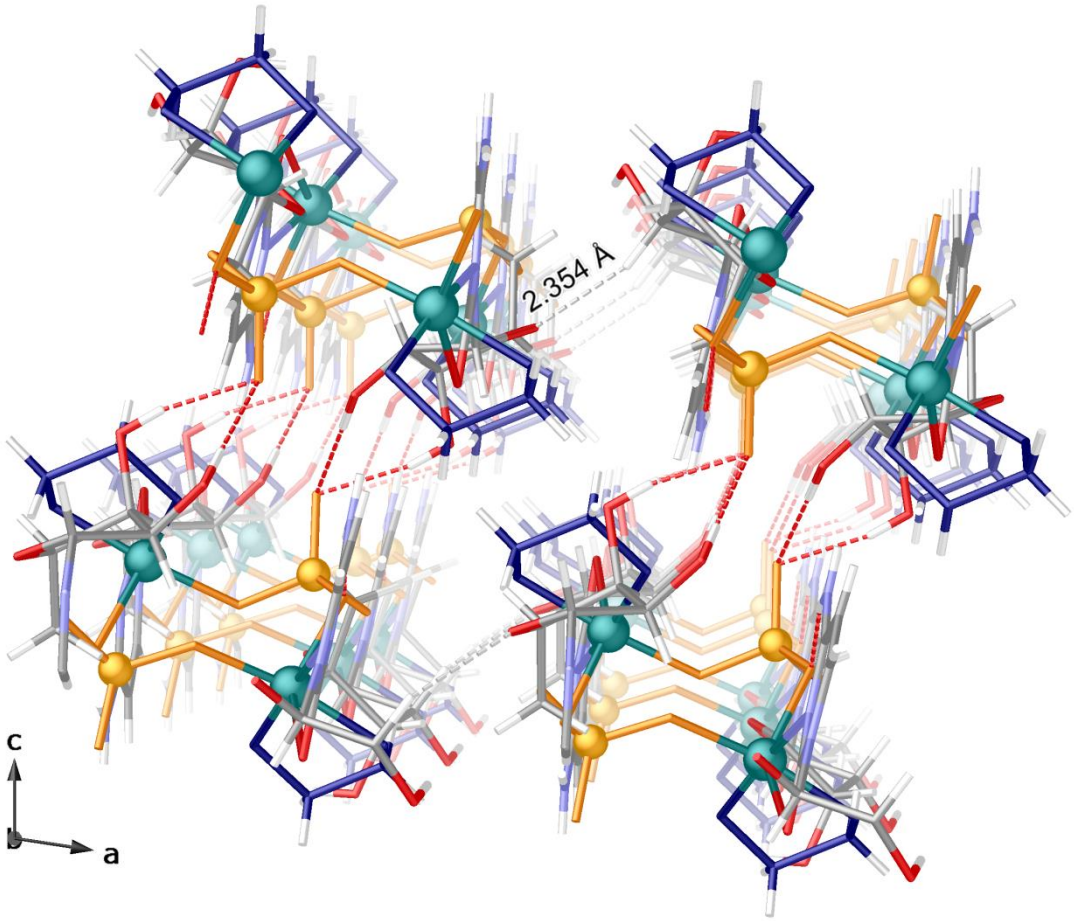

Figure 6. Perspective view down *b* axes showing adjacent $\{[Cu_2(en)_2(CMP)_2\}_n$ supramolecular chains weakly interacting by means of interactions established between hydroxyl groups and alkyl residues of ethylendiammine, pointing towards voids, of the type H-O···H-C [O···H distance of 2.36(1) Å. Color sticks legend: C, gray; N, light blue; O, red; H, white; Carbon and nitrogen atoms from ethylndiammine ligand have been depicted in blue whereas oxygen atoms of phosphate groups are depicted in gold for the sake of clarity.

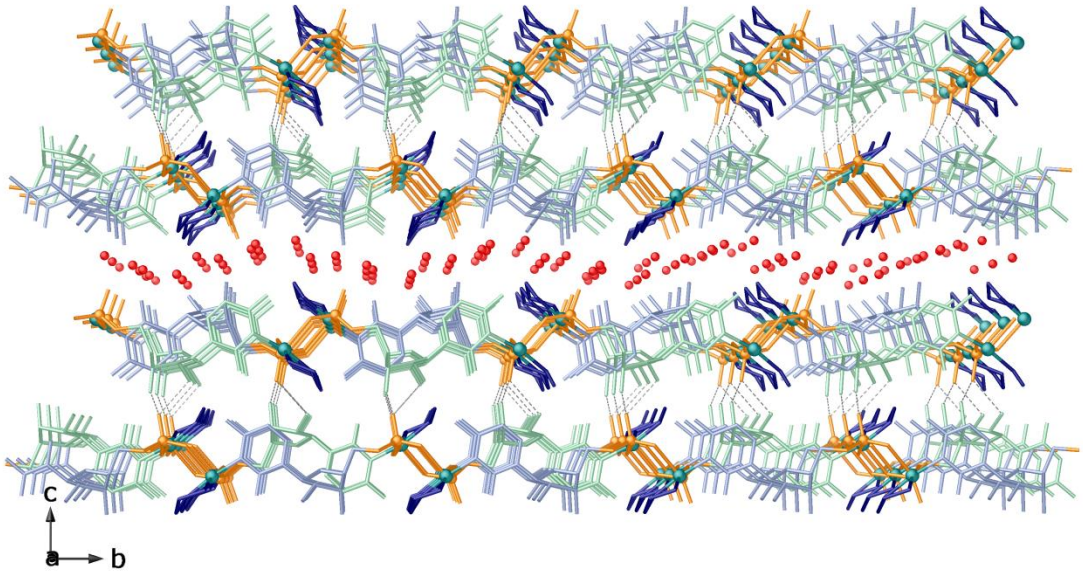

Figure 7. Perspective view of crystal packing in **1** showing supramolecular chains (generated by strong and symmetric hydrogen bonding interactions involving hydroxyl groups from ribose and phosphate from CMP) stacked in the *ab* plane and intercalated by lattice water molecules (red spheres). Crystallographically distinct CMP Color have been depicted as light green and light blue sticks; Carbon and nitrogen atoms from ethylndiammine ligand have been depicted in blue whereas oxygen atoms of phosphate groups are depicted in gold for the sake of clarity.

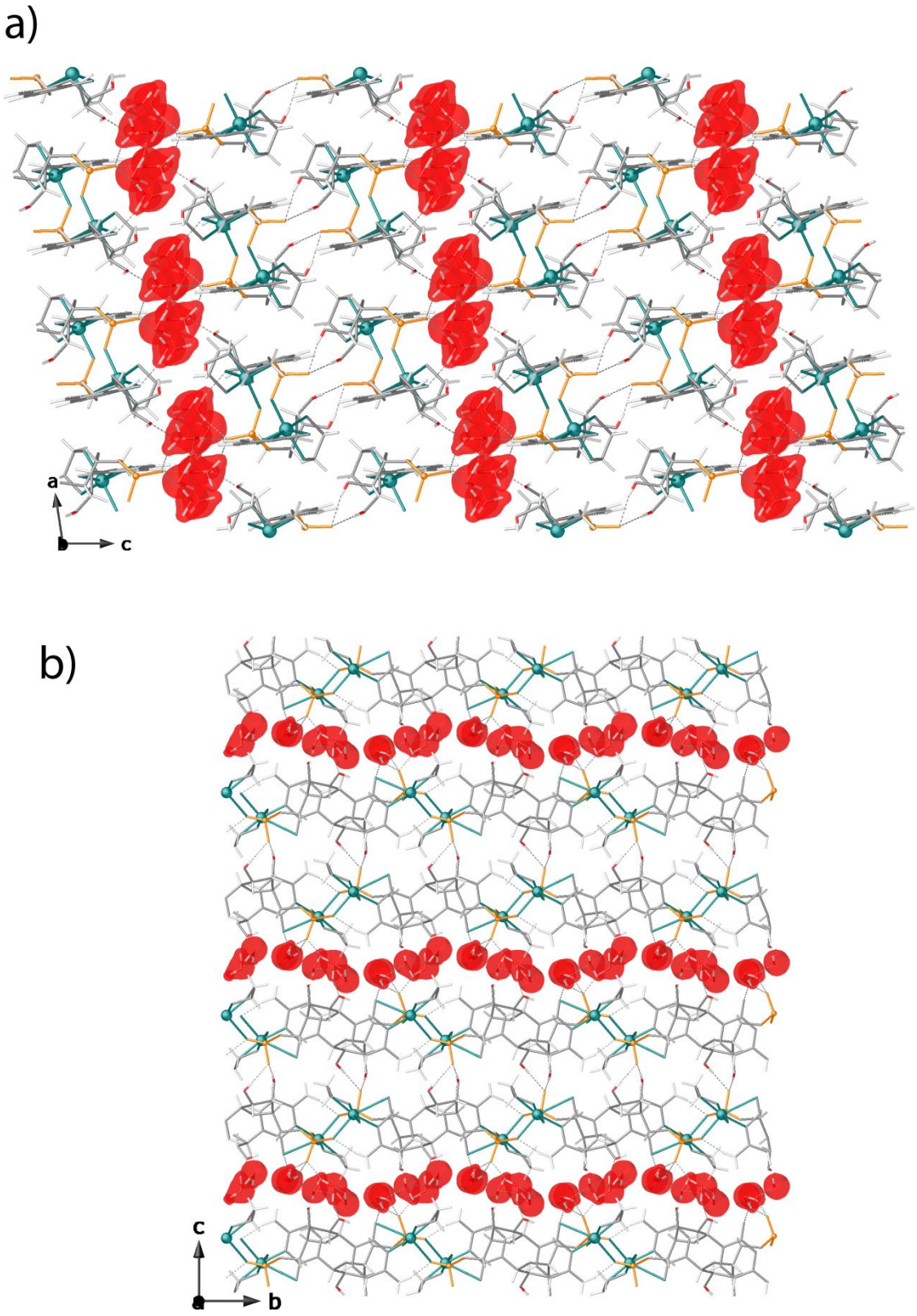

Figure 8. Views down the *b* and *a* crystallographic axes of overall packing of supramolecular chains creating a porous structure with small pores filled by water molecules (red spheres highlighted with surface underline the solvent accessible voids). Color sticks legend: C, gray; N, light blue; O, red; H, white. Oxygen atoms of phosphate groups are depicted in gold for the sake of clarity.

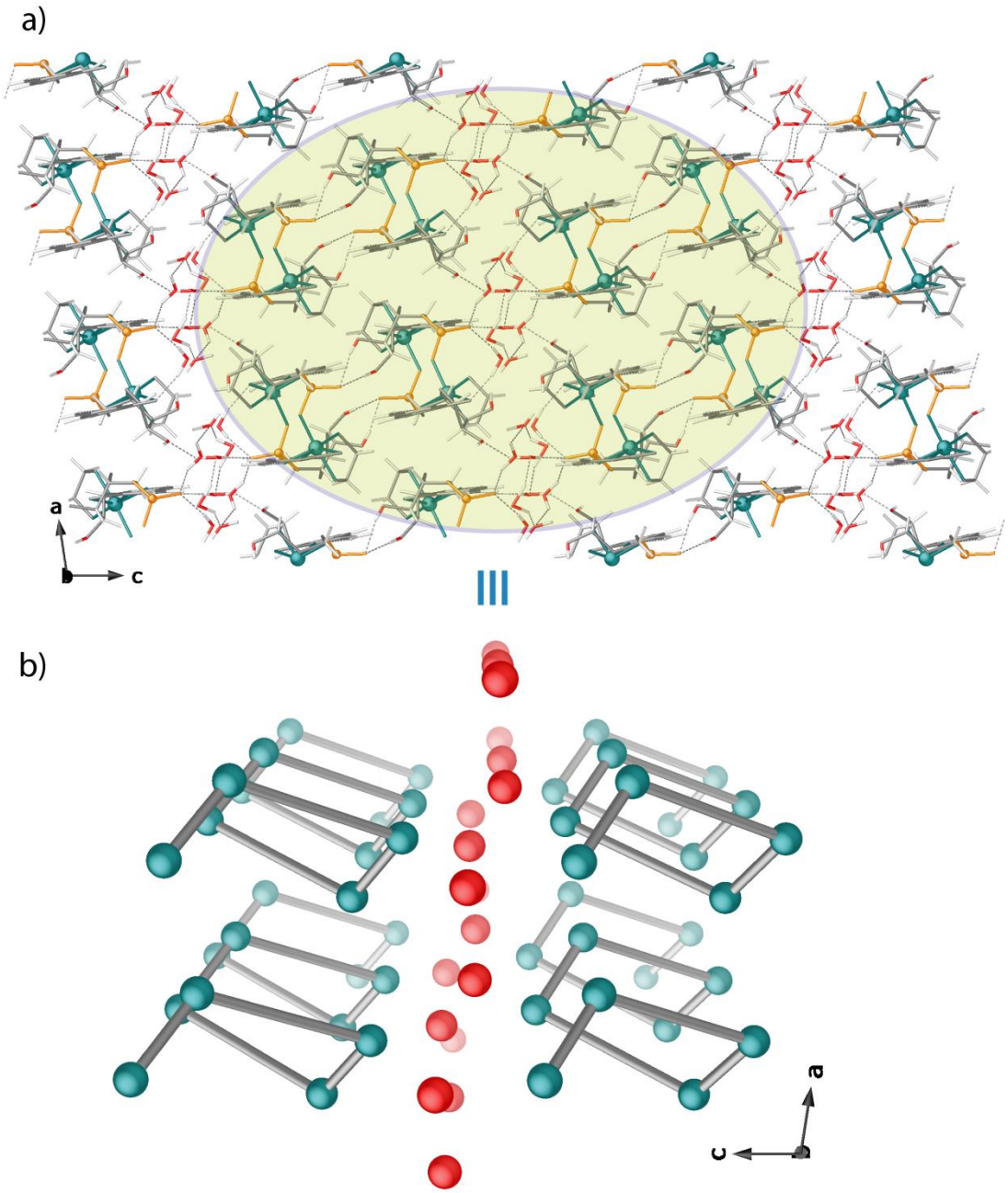

Figure 9. View of portion of supramolecular chains in **1** and its deconstruction to simple copper rod geometries (a and b, respectively). The $\{[Cu_2(en)_2(CMP)_2\}_n$ chains are connected *via* hydrogen bonds to construct a 2_1 helix. Then these two-fold helices of *P* handness are packed *via* further interactions to generate a porous 3D HMOF. Copper ions and lattice water molecules are depicted by green and red spheres, respectively.

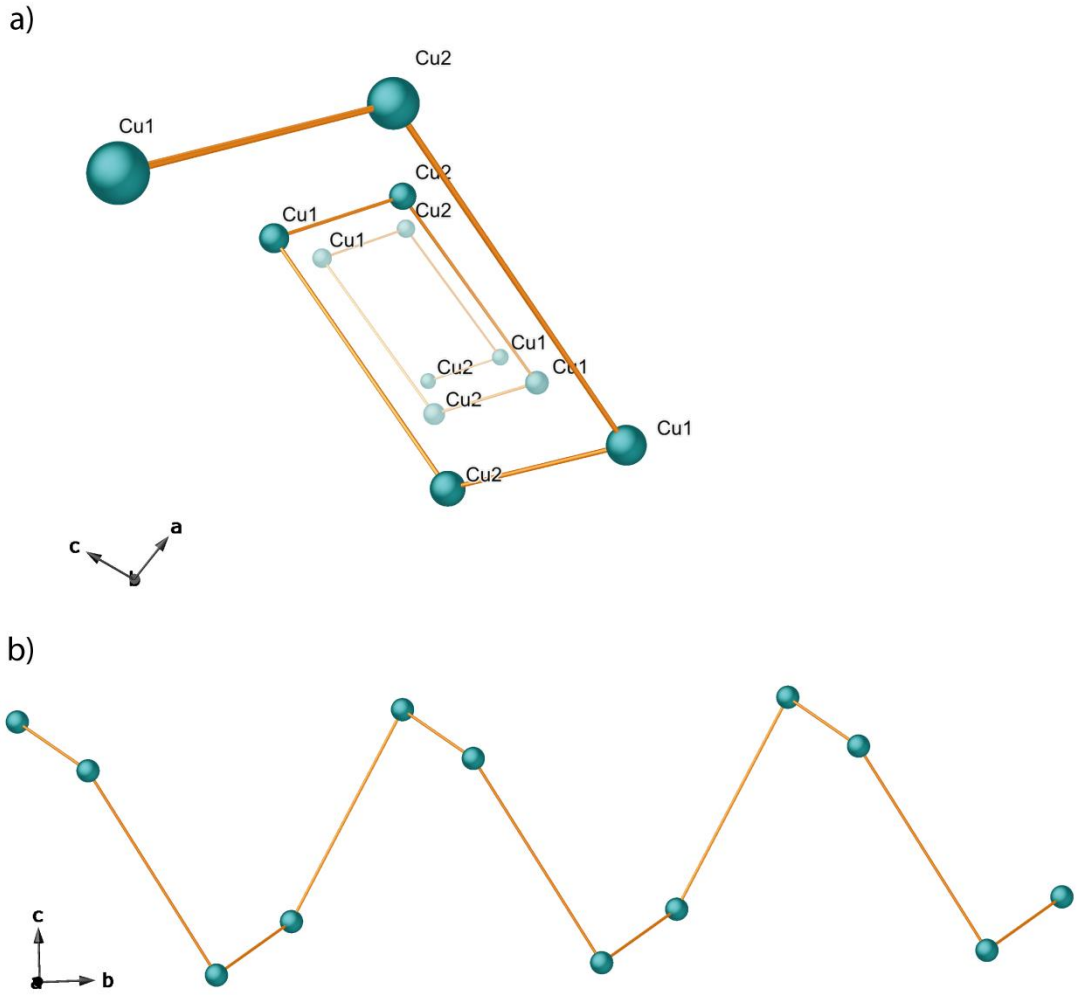

Figure 10. (a) Top and (b) side schematic representation of $\{[Cu_2(en)_2(CMP)_2\}_n$ right-handed helices with helical pitch of 13.259 Å supramolecular chains.

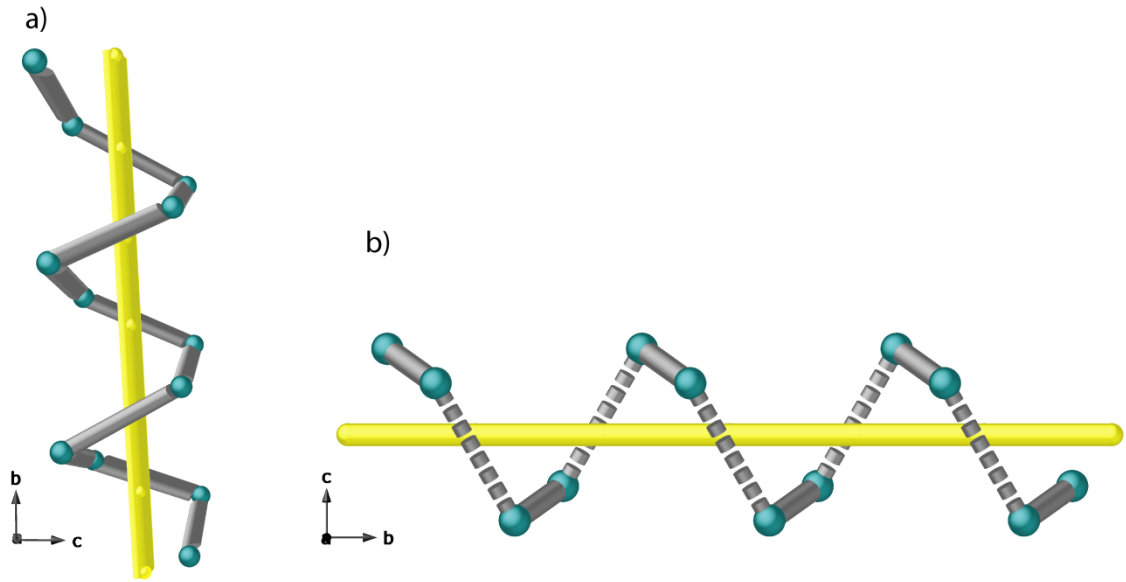

Figure 11. Handness *P* exhibited by supramolecular chain built in **1**: perspective views along *a* and *b* crystallographic axis, respectively shown in a) and b).